Biomechanics and Modeling in Mechanobiology manuscript No.

Modeling cell apoptosis for simulating three-dimensional multicellular morphogenesis based on a reversible network reconnection framework

Satoru Okuda · Yasuhiro Inoue · Mototsugu Eiraku · Taiji Adachi · Yoshiki Sasai

Received: 10 June 2015 / Accepted: 25 August 2015 / Published online: 11 September 2015

Abstract Morphogenesis in multicellular organisms is accompanied by apoptotic cell behaviors: cell shrinkage and cell disappearance. The mechanical effects of these behaviors are spatiotemporally regulated within multicellular dynamics to achieve proper tissue sizes and shapes in three-dimensional (3D) space. To analyze 3D multicellular dynamics, 3D vertex models have been suggested, in which a reversible network reconnection (RNR) model has successfully expressed 3D cell rearrangements during large deformations. To analyze the effects of apoptotic cell behaviors on 3D multicellular morphogenesis, we modeled cell apoptosis based on the RNR model framework. Cell shrinkage was modeled by the potential energy as a function of individual cell times during the apoptotic phase. Cell disappearance was modeled by merging neighboring polyhedrons at their boundary surface according to the topological rules of the RNR model. To establish that the apoptotic cell behaviors could be expressed as modeled, we simulated morphogenesis driven by cell apoptosis in two types of tissue topology: 3D monolayer cell sheet and 3D compacted cell aggregate. In both types of tissue topology, the numerical simulations successfully illustrated that cell aggregates gradually shrank because of successive cell apoptosis. During tissue shrinkage, the number of cells in aggregates decreased while maintaining individual cell size and shape. Moreover, in case of localizing apoptotic cells within a part of the 3D monolayer cell aggregate, the cell apoptosis caused the global tissue bending by pulling on surrounding cells. In case of localizing apoptotic cells on the surface of the 3D compacted cell aggregate, the cell apoptosis caused successive, directional cell rearrangements from the inside to the surface. Thus, the proposed model successfully provided a basis for expressing apoptotic cell behaviors during 3D multicellular morphogenesis based on an RNR model framework.

Keywords Multicellular morphogenesis · Cell apoptosis · Apoptotic force · Three-dimensional vertex model · Reversible network reconnection model · Computational biomechanics

S. Okuda · M. Eiraku
Laboratory for *in vitro* Histogenesis, Center for Developmental Biology (CDB), RIKEN, 2-2-3 Minatojima-minamimachi, Chuo-ku, Kobe, Hyogo, 650-0047, Japan
E-mail: okuda@cdb.riken.jp

S. Okuda · Y. Sasai
Laboratory for Organogenesis and Neurogenesis, Center for Developmental Biology (CDB), RIKEN, Kobe, Japan

Y. Inoue · T. Adachi
Department of Biomechanics, Institute for Frontier Medical Sciences, Kyoto University, Japan

1 Introduction

During multicellular morphogenesis, the number of cells is spatiotemporally regulated, and cell apoptosis has a crucial role in decreasing the number of cells to form three-dimensional (3D) structures of several tissues and organs. Because the size of each cell is approximately maintained during short periods of individual developmental stages, the size of the whole tissue efficiently decreases. For example, cell apoptosis is characteristically located at the lateral edges of the hindbrain neural tube prior to closure in wild-type embryos, but this activity is greatly reduced in mouse mutants (Kuan et al. 2000; Yamaguchi et al 2011). Because of this reduction in region-specific apoptosis, embryos of the mouse mutants exhibited neurulation defects in the hindbrain. The necessity of cell apoptosis in morphogenesis has

also been reported in several tissues, e.g., the inner ear (Fekete et al. 1997), optic-cup (Trousse et al. 2001), brain, (Kuan et al. 2000), limb bud (Suzanne and Steller 2013), and heart (Zhao and Rivkees 2000). In morphogenesis, the timing and region of cell apoptosis are specific. Thus, apoptotic cell behaviors have important roles in 3D multicellular morphogenesis.

Recent studies suggested several mechanical roles of apoptotic cell behaviors in morphogenesis. In Drosophila embryogenesis, the expression of proteins that suppress or enhance apoptosis slows or speeds dorsal closure, respectively. These changes correlate with the cell mechanical states and the rate of closure (Toyama et al. 2008). In the dorsal closure, it has been also reported that the decrease in cell volume is triggered by caspase activation and generates contractile forces that promote tissue shrinkage (Saias et al. 2015). Moreover, genitalia rotation is relatively impaired by reducing the activity of caspase signaling (Kuranaga et al. 2011). In addition, apoptotic cells generate a transient pulling force on the apical surface of the epithelium through an apico-basal myosin II cable, which is lost in the absence of apoptosis (Monier et al. 2015). These mechanical effects of apoptotic cell behaviors are spatiotemporally regulated to achieve proper tissue and organ morphology.

During these events of morphogenesis accompanied by apoptotic cell behaviors, multicellular dynamics is commonly observed, such as cell deformation and rearrangement (Davies 2005; Farhadifar et al. 2007; Ingber and Mammoto 2010; Rauzi et al. 2008; Staple et al. 2010; Weliky and Oster 1990; Lecuit and Lenne 2007; Lecuit et al. 2010; Friedlander et al. 1989; Lecuit et al. 2008). This multicellular dynamics is necessary for forming the 3D complex structures of tissues and organs. Hence, to obtain a better understanding of morphogenesis, it is necessary to determine the mechanical effects of apoptotic cell behaviors on 3D multicellular dynamics.

To analyze 3D multicellular dynamics, 3D vertex models have been proposed (Honda et al. 2004, 2008a,b; Okuda et al. 2013a,b,c, 2015a,b). In 3D vertex models, the shape of each cell is represented by a single polyhedron, and a 3D cell aggregate is represented by a single network comprising vertices and edges. In addition, cell deformations are expressed by vertex dynamics, and cell rearrangements are expressed by reconnecting local network patterns. A 3D vertex model (Honda et al. 2004) has been successfully used to analyze the polarization of early embryos (Honda et al. 2008a) and convergent extensions of epithelium (Honda et al. 2008b). In addition, to ensure physical consistency in the 3D vertex model, a reversible network reconnection (RNR) model has been proposed (Okuda et al. 2013a, 2015b). By improving the rule of the network reconnections, the RNR model has succeeded in simulating large 3D deformations with frequent cell rearrangements. Thus, modeling cell apoptosis on a 3D vertex model framework will give a powerful tool to investigate the mechanical effects of cell apoptosis on 3D multicellular morphogenesis.

Modeling cell apoptosis requires expressing apoptotic cell behaviors: cell shrinkage (decrease in cell volume) and cell disappearance (decrease in cell number) according to the employed conditions. In particular, modeling the cell disappearance requires reconnecting topological patterns of the vertex network. However, the network reconnection can possibly produce several irreversible patterns for cell rearrangements, which arrest the network topology (Okuda et al. 2013a). This topological error is inadmissible for performing computational simulations because it could generate artificial forces or stop the calculations. Hence, to simulate morphogenesis with successive cell apoptosis using the 3D vertex model, apoptotic cell behaviors should be expressed while maintaining the topological reversibility of the vertex network. To satisfy the topological reversibility, one possible method is to employ the topological rules of network reconnections in the RNR model.

In this study, to analyze the mechanical effects of apoptotic cell behaviors on 3D multicellular morphogenesis, we model cell apoptosis according to the topological rules of network reconnections in the RNR model. To demonstrate the applicability of the proposed model, we applied it to simulate morphogenesis driven by homogeneous and region-specific cell apoptosis. By simulating apoptosis-driven tissue shrinkage, we establish whether apoptotic cell behaviors could be recapitulated by the proposed model. Based on these results, applicability and future perspectives of the proposed model have also been discussed.

2 Modeling 3D cell apoptosis based on an RNR framework

2.1 Dynamics of 3D cell aggregates

Most tissues and organs have a 3D multicellular structure, within which individual cells are tightly compacted and adhered to neighboring cells. The RNR model (Okuda et al. 2013a) expresses a single cell shape using a polyhedron (Figs. 1a and b). Individual polyhedrons include vertices and edges that are shared by neighboring polyhedrons. These vertices and edges comprise a network that represents the entire shape of the aggregate (Figs. 1c and d). In this network, each vertex is connected to exactly four edges. In addition, neighboring polyhedrons are compartmentalized by these polygonal faces.

The dynamics of cell aggregates is expressed by an equation for the motion of the i^{v}th vertex (Okuda et al. 2015a) as follows:

$$\eta_{i^{\mathrm{v}}}\left(\frac{d\boldsymbol{r}_{i^{\mathrm{v}}}}{dt}-\boldsymbol{v}_{i^{\mathrm{v}}}\right)=-\frac{\partial U}{\partial \boldsymbol{r}_{i^{\mathrm{v}}}}. \tag{1}$$

The left-hand side of Eq. (1) indicates a frictional force exerted on the i^{v}th vertex. Scalar $\eta_{i^{\mathrm{v}}}$ is a friction coefficient, and $\boldsymbol{r}_{i^{\mathrm{v}}}$ is the position vector of the i^{v}th vertex. Vector $\boldsymbol{v}_{i^{\mathrm{v}}}$ is the local velocity at the i^{v}th vertex. The right-hand side of Eq. (1) denotes potential force acting on the i^{v}th vertex, where U is potential energy. In addition, cell rearrangements within an aggregate are expressed by reconnecting local network patterns (Okuda et al. 2013a).

2.2 Apoptotic cell behaviors

Apoptotic cell behaviors are characterized by cell shrinkage and disappearance (Figs. 1c and e). Based on the RNR model framework, these apoptotic cell behaviors should be expressed from two perspectives: physical and topological (Figs. 1d and f). From the physical perspective, cell shrinkage can be expressed by a potential energy function (Figs. 1g and h). From the topological perspective, because a single cell is represented by a single polyhedron based on the RNR model framework, a polyhedron is eliminated by merging it with the neighboring polyhedron (Figs. 1h and i). Thus, we have provided separate physical and topological models of cell apoptosis.

First, for the physical modeling of cell apoptosis, cell time $t_{j^{\mathrm{c}}}$ is defined as a real number counted as $t_{j^{\mathrm{c}}}=0$ when the j^{c}th cellular polyhedron was generated. The apoptotic cell behaviors are defined by two parameters for each cell: $t_{j^{\mathrm{c}}}^{\mathrm{ps}}$ and $t_{j^{\mathrm{c}}}^{\mathrm{dis}}$ $(0<t_{j^{\mathrm{c}}}^{\mathrm{ps}}<t_{j^{\mathrm{c}}}^{\mathrm{dis}})$, wherein the j^{c}th cell shifts its phase from stable to apoptotic at $t_{j^{\mathrm{c}}}=t_{j^{\mathrm{c}}}^{\mathrm{ps}}$, and the j^{c}th cell disappears at $t_{j^{\mathrm{c}}}=t_{j^{\mathrm{c}}}^{\mathrm{dis}}$. Hence the j^{c}th cellular polyhedron exists in the range of $0\leq t_{j^{\mathrm{c}}}\leq t_{j^{\mathrm{c}}}^{\mathrm{dis}}$.

Defining $\{t_{j^{\mathrm{c}}}\}=\{t_{0^{\mathrm{c}}},t_{1^{\mathrm{c}}},t_{2^{\mathrm{c}}},\cdots,t_{3^{\mathrm{c}}},\cdots,t_{n^{\mathrm{c}}}\}$, the potential energy $U(\{t_{j^{\mathrm{c}}}\})$ was introduced as a function of cell time $\{t_{j^{\mathrm{c}}}\}$ within the particular apoptotic phase. Using cell time $t_{j^{\mathrm{c}}}$, potential energy, U, is expressed by

$$U=U^{\mathrm{cell}}+U^{\mathrm{cell\text{–}cell}}+U^{\mathrm{cell\text{–}ext}}, \tag{2}$$

$$U^{\mathrm{cell}}=\sum_{j^{\mathrm{c}}}^{\mathrm{cell}}u_{j^{\mathrm{c}}}^{\mathrm{cell}}\left(\boldsymbol{r}_{i^{\mathrm{v}}},t_{j^{\mathrm{c}}}\right)\delta_{j^{\mathrm{c}}}^{*}, \tag{3}$$

$$U^{\mathrm{cell\text{–}cell}}=\sum_{j^{\mathrm{c}}}^{\mathrm{cell}}\sum_{k^{\mathrm{c}}}^{\mathrm{cell}}u_{j^{\mathrm{c}}k^{\mathrm{c}}}^{\mathrm{cell\text{–}cell}}\left(\boldsymbol{r}_{i^{\mathrm{v}}},t_{j^{\mathrm{c}}},t_{k^{\mathrm{c}}}\right)\delta_{j^{\mathrm{c}}}^{*}\delta_{k^{\mathrm{c}}}^{*}, \tag{4}$$

$$U^{\mathrm{cell\text{–}ext}}=\sum_{j^{\mathrm{c}}}^{\mathrm{cell}}u_{j^{\mathrm{c}}}^{\mathrm{cell\text{–}ext}}\left(\boldsymbol{r}_{i^{\mathrm{v}}},t_{j^{\mathrm{c}}}\right)\delta_{j^{\mathrm{c}}}^{*}, \tag{5}$$

where $\delta_{j^{\mathrm{c}}}^{*}=\delta_{\lfloor t_{j^{\mathrm{c}}}/t_{j^{\mathrm{c}}}^{\mathrm{dis}}\rfloor 0}$. The functions $\delta_{\alpha\beta}$ and $\lfloor ...\rfloor$ indicate Kronecker's delta and floor functions, respectively. In Eqs. (3), (4), and (5), $\sum^{\mathrm{cell}}$ indicates summations for all cells. Potential energy $u_{j^{\mathrm{c}}}^{\mathrm{cell}}$ represents an energy of the j^{c}th cell, such as volume elasticity, surface elasticity, apical constriction, and other effects of intracellular structures and activities. The potential energy $u_{j^{\mathrm{c}}k^{\mathrm{c}}}^{\mathrm{cell\text{–}cell}}$ indicates energy between the j^{c}th and k^{c}th cells, such as cell-cell adhesions at intercellular junctions. The potential energy $u_{j^{\mathrm{c}}}^{\mathrm{cell\text{–}ext}}$ indicates energy between the j^{c}th cell and extracellular components, such as extracellular matrixes, basement membranes, and solvent liquids. In this model, cell shrinkage is expressed by time-variations in the constants of Eqs. (3, 4, 5) such as mechanical property, the reference state, and energy density.

Second, for the topological modeling of cell apoptosis, each polyhedron is eliminated by merging it to the neighboring polyhedron (Figs. 1h and i). Before merging polyhedrons, the polyhedron expressing the apoptotic cell neighbors the other polyhedron across their boundary polygon (Fig. 1h). The boundary polygon is composed of several edges that are sequentially linked as a ring-like strand. Each of these edges also comprises a couple of other polygons that compose the apoptotic and neighboring polyhedrons, respectively. By removing the boundary polygon, individual couples of polygons are merged into single polygons (Fig. 1i).

To perform numerical simulations with 3D cell rearrangements, the network should satisfy the reversibility of the network reconnection as described by (Okuda et al. 2013a). To satisfy the reversibility, the network reconnection of the apoptosis proceeds according to the following rules:

i. Two edges never share two vertices simultaneously.
ii. Two polygonal faces never share two or more edges simultaneously.

These topological rules are the same as those of the RNR model that is proposed for expressing 3D cell rearrangements (Okuda et al. 2013a).

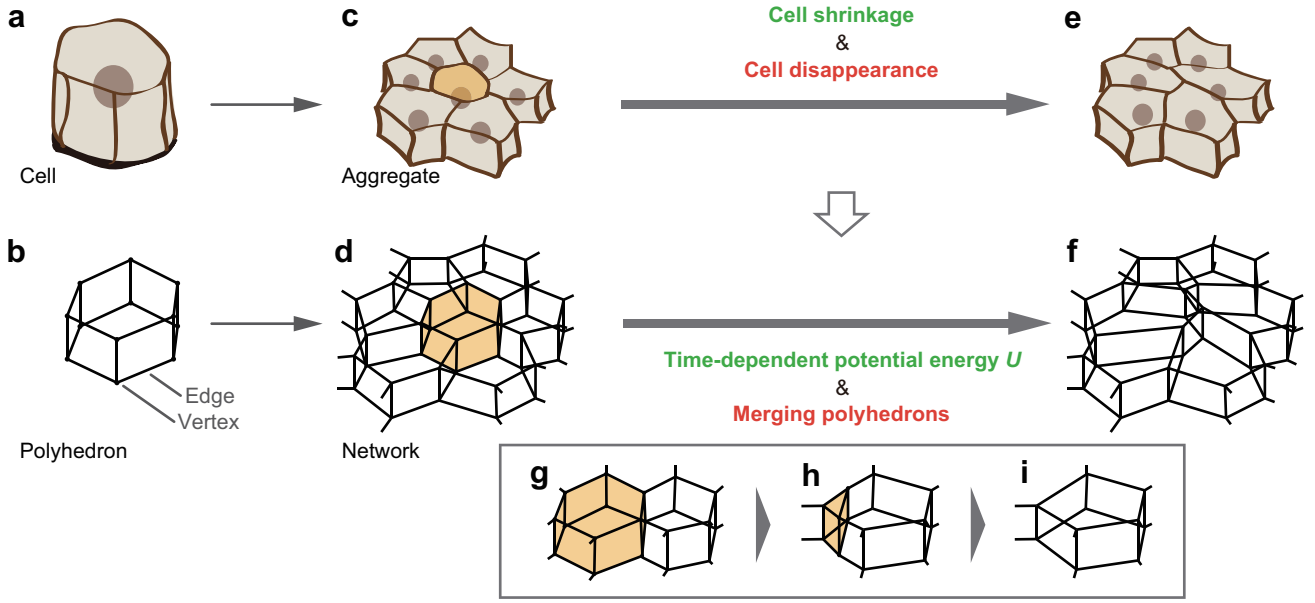

Fig. 1 Modeling of cell apoptosis based on an RNR framework. **a** Individual cells. **b** Polyhedrons expressing individual cells. **c** Cell aggregate within which cells are tightly compacted and adhered at cell–cell boundaries. **d** Network representing a cell aggregate in an RNR model framework. The network comprises vertices and edges. Cells are compartmentalized by polygonal faces that represent cell–cell boundaries. **e** Cell aggregate within which the yellow cell colored in (**c**) disappeared via apoptosis. **f** Network representing a cell aggregate within which the yellow polyhedron colored in (**d**) disappeared. **g**, **h**, **i** The process of merging polyhedrons. The yellow polyhedron shrinks during the apoptotic phase from (**g**) to (**h**), which is expressed by potential energy as a function of individual cell times, U. In the disappearance process from (**h**) to (**i**), the yellow polyhedron merges with the neighboring polyhedron.

From a numerical standpoint, merging polyhedrons causes the artificial drift of cellular locations. To suppress the drift, the polyhedron whose centroid is the closest to that of the apoptotic polyhedron is merged into the apoptotic polyhedron. Moreover, to minimize the drift, locations of the vertices composing apoptotic cells are modified to maintain the centroid of surrounding cellular population. When the j^{c}th cell disappears by merging polyhedrons on the l^{s}th surface, the i^{v}th vertex location after the modification, represented by $\boldsymbol{r}_{i^{\mathrm{v}}}^{\mathrm{mod}}$, is written as follows.

$$\boldsymbol{r}_{i^{\mathrm{v}}}^{\mathrm{mod}} = \boldsymbol{r}_{i^{\mathrm{v}}} + \left(\frac{\sum_{i^{\mathrm{v}}}^{\mathrm{vertex}} \boldsymbol{r}_{i^{\mathrm{v}}} \delta_{i^{\mathrm{v}};j^{\mathrm{c}}}}{\sum_{i^{\mathrm{v}}}^{\mathrm{vertex}} \delta_{i^{\mathrm{v}};j^{\mathrm{c}}}} - \frac{\sum_{i^{\mathrm{v}}}^{\mathrm{vertex}} \boldsymbol{r}_{i^{\mathrm{v}}} \delta_{i^{\mathrm{v}};j^{\mathrm{c}}} - \sum_{k^{\mathrm{v}}}^{\mathrm{vertex}} \boldsymbol{r}_{k^{\mathrm{v}}} \delta_{k^{\mathrm{v}};l^{\mathrm{s}}}}{\sum_{i^{\mathrm{v}}}^{\mathrm{vertex}} \delta_{i^{\mathrm{v}};j^{\mathrm{c}}} - \sum_{k^{\mathrm{v}}}^{\mathrm{vertex}} \delta_{k^{\mathrm{v}};l^{\mathrm{s}}}} \right), \tag{6}$$

where binary function $\delta_{i^{\mathrm{v}};j^{\mathrm{c}}}$ is 1 if the j^{c}th cell contains the i^{v}th vertex and 0 otherwise. The binary function $\delta_{k^{\mathrm{v}};l^{\mathrm{s}}}$ is 1 if the l^{s}th surface contains the k^{v}th vertex and 0 otherwise.

3 Introducing cell behaviors into the proposed model

To demonstrate the applicability of the proposed model, apoptosis-driven morphogenesis was simulated in two cases using the 3D monolayer cell sheet and the 3D compacted cell aggregate. Moreover, by focusing on effects of the decrease in cell volume, as observed in Drosophila dorsal closure (Saias et al. 2015), we observed cell shape, size, configuration, and 3D tissue morphology. For these simulations, apoptotic cell behaviors and the potential energy are simply expressed as follows.

3.1 Apoptotic cell behaviors

In the proposed model, apoptotic cell behaviors are determined by regulations of the timing $t_{j^{\mathrm{c}}}^{\mathrm{ps}}$ and $t_{j^{\mathrm{c}}}^{\mathrm{dis}}$ as described in Section 2.2. To demonstrate the simulations using the proposed model, the timing of the phase shift from stable to apoptotic $t_{j^{\mathrm{c}}}^{\mathrm{ps}}$ was randomly determined to satisfy the half-life period of τ^{hl}. In addition, by introducing the time period of the apoptotic phase τ^{ap}, the timing of the cell disappearance $t_{j^{\mathrm{c}}}^{\mathrm{dis}}$ is determined to be $t_{j^{\mathrm{c}}}^{\mathrm{dis}} = t_{j^{\mathrm{c}}}^{\mathrm{ps}} + \tau^{\mathrm{ap}}$. The parameters τ^{hl} and τ^{ap} were determined to be constant, independent of the cell mechanical state. Under this condition, the decreases in

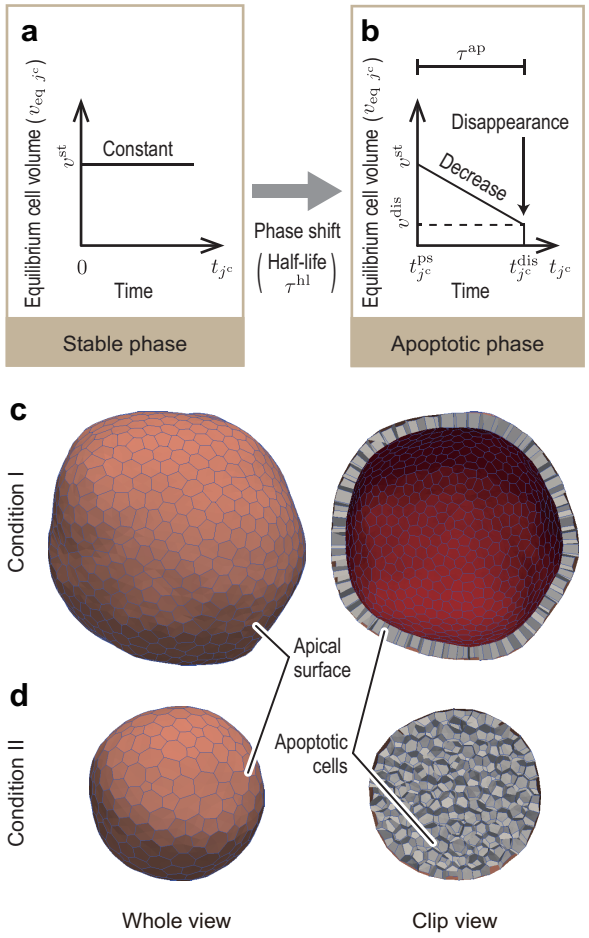

Fig. 2 Introducing apoptotic cell behaviors into the proposed model as an example. **a**, **b** Equilibrium cell volume as a function of individual cell times in the stable and apoptotic phases, respectively. Cells randomly shift their phases from stable (**a**) to apoptotic (**b**) to satisfy the half-life period of τ^{hl}. Equilibrium volume of the j^{c}th cell as a function of the j^{c}th cell time, denoted by $v_{\mathrm{eq}\ j^{\mathrm{c}}}\left(t_{j^{\mathrm{c}}}\right)$, as described by Eq. (10). In the stable phase (**a**), cell equilibrium volume is constant. In the stable phase (**b**), cell equilibrium volume decreases linearly with time. The j^{c}th cell disappears at $t_{j^{\mathrm{c}}}^{\mathrm{dis}} = t_{j^{\mathrm{c}}}^{\mathrm{ps}} + \tau^{\mathrm{ap}}$. **c** Whole and clip views of the initial structure of the cell aggregate under condition I. The cell aggregate has a structure of spherical shell composed of 3D monolayer cell sheet, where all cells (light gray) shift their phases from stable to apoptotic. **d** Whole and clip views of the initial structure of the cell aggregate under condition II. The cell aggregate has a spherical structure composed of 3D compacted cells, where all cells (light gray) shift their phases from stable to apoptotic. In (**c**) and (**d**), the outside surfaces of the individual cell aggregates (orange) are apical.

the number of cells obeyed the theoretical solution as follows.

$$n^{\mathrm{c}}\left(t\right) = n_0^{\mathrm{c}} \cdot \left(\frac{1}{2}\right)^{t/\tau^{\mathrm{hl}}}, \tag{7}$$

where n_0^{c} indicates the number of cells under the initial condition.

3.2 Cell potential energy

To determine whether apoptotic cell behaviors could be recapitulated as modeled, we simply supposed the cell behaviors to maintain their size and shape as an example. Cell potential energy was simply expressed using the potential energy by

$$U^{\mathrm{total}} = U^{\mathrm{cv}} + U^{\mathrm{cs}} + U^{\mathrm{aj}}, \tag{8}$$

where U^{cv} is cell volume elasticity, U^{cs} is cell surface energy, and U^{aj} is tensile energy at the adherence junction. Here, U^{cv} and U^{cs} are categorized by U^{cell}, and U^{aj} is categorized by $U^{\mathrm{cell\text{–}cell}}$ in Eq. (2).

3.2.1 Cell volume elasticity

To express cell volume elasticity, the current volume of the j^{c}th cell, $v_{j^{\mathrm{c}}}\left(t_{j^{\mathrm{c}}}\right)$, was introduced. Then, cell volume elasticity, U^{cv}, was expressed by

$$U^{\mathrm{cv}} = \sum_{j^{\mathrm{c}}}^{\mathrm{cell}} \frac{1}{2} k^{\mathrm{cv}} \left(\frac{v_{j^{\mathrm{c}}}}{v_{\mathrm{eq}\ j^{\mathrm{c}}}} - 1\right)^2, \tag{9}$$

where $\sum_{j^{\mathrm{c}}}^{\mathrm{cell}}$ indicates the summation for all cells. The constant k^{cv} indicates volume elasticity. The variable $v_{\mathrm{eq}\ j^{\mathrm{c}}}$ indicates an equilibrium volume of the j^{c}th cell as a function of the j^{c}th cell time $t_{j^{\mathrm{c}}}$.

The equilibrium cell volume of the j^{c}th cell $v_{\mathrm{eq}\ j^{\mathrm{c}}}$ is constant in the stable phase (Fig. 2a), while it decreases linearly according to the j^{c}th cell time $t_{j^{\mathrm{c}}}$ in the apoptotic phase (Fig. 2b):

$$v_{\mathrm{eq}\ j^{\mathrm{c}}}\left(t_{j^{\mathrm{c}}}^{\mathrm{ap}}\right) = \begin{cases} v^{\mathrm{st}} & \text{in stable phase} \\ v^{\mathrm{st}}\left(1 - \gamma_{j^{\mathrm{c}}}\right) + v^{\mathrm{dis}}\gamma_{j^{\mathrm{c}}} & \text{in apoptotic phase} \end{cases}, \tag{10}$$

where $\gamma_{j^{\mathrm{c}}} = \left(t_{j^{\mathrm{c}}} - t_{j^{\mathrm{c}}}^{\mathrm{ps}}\right)/\tau^{\mathrm{ap}}$. The constants v^{st} and v^{dis} indicate a characteristic cell volume and apoptotic cell volume, respectively.

3.2.2 Cell surface energy

To express cell surface energy, a current surface of the j^{c}th cell, $s_{j^{\mathrm{c}}}\left(t_{j^{\mathrm{c}}}\right)$, was introduced. Then, cell surface energy, U^{cs}, was expressed by

$$U^{\mathrm{cs}} = \sum_{j^{\mathrm{c}}}^{\mathrm{cell}} \kappa^{\mathrm{cs}} s_{j^{\mathrm{c}}}, \tag{11}$$

where the constant κ^{cs} indicates surface energy density.

3.2.3 Tensile energy on adherence junction

Adherence junctions are defined on the all edges on the surface of the aggregate. When cells move into the inside of the aggregate, they lose their adherence junctions along with losing their edges on the surface. Conversely, when cells move to the surface, they obtain their adherence junctions along with obtaining their edges on the surface. To express tensile energy on adherence junctions, a current length of the edge on the apical surface between the j^{c}th cell and k^{c}th cells, $l^{\mathrm{a}}_{j^{\mathrm{c}}k^{\mathrm{c}}}(t_{j^{\mathrm{c}}})$, was introduced on the apical surface. Then, the tensile energy on adherence junctions, U^{aj}, was expressed by

$$U^{\mathrm{aj}} = \sum_{j^{\mathrm{c}}}^{\mathrm{cell}} \sum_{k^{\mathrm{c}}>j^{\mathrm{c}}}^{\mathrm{cell}} \kappa^{\mathrm{aj}} l^{\mathrm{a}}_{j^{\mathrm{c}}k^{\mathrm{c}}}, \tag{12}$$

where the constant κ^{aj} indicates line energy density. The binary function $\delta_{i^{\mathrm{v}};j^{\mathrm{e}}}$ is 1 if the j^{e}th geometric element contains the i^{v}th vertex and 0 otherwise. Equations (9), (11), and (12) are similar to those employed in studies of other vertex models (Farhadifar et al. 2007; Honda et al. 2004, 2008a,b).

3.3 Cellular viscous frictions

The friction coefficient $\eta_{i^{\mathrm{v}}}$ and local velocity $\boldsymbol{v}_{j^{\mathrm{e}}}$ are defined as described in a previous study (Okuda et al. 2015a) as follows.

The viscous friction coefficient $\eta_{i^{\mathrm{v}}}$ in Eq. (1) is simply defined as follows

$$\eta_{i^{\mathrm{v}}} = \sum_{j^{\mathrm{e}}}^{\mathrm{element}} \eta_{j^{\mathrm{e}}} \delta_{i^{\mathrm{v}};j^{\mathrm{e}}}, \tag{13}$$

where $\sum_{j^{\mathrm{e}}}^{\mathrm{element}}$ is the summation of the overall geometric elements. The binary function $\delta_{i^{\mathrm{v}};j^{\mathrm{e}}}$ is 1 if the j^{e}th geometric element contains the i^{v}th vertex and 0 otherwise. The constant $\eta_{j^{\mathrm{e}}}$ is the viscous friction weight of vertices in the j^{e}th geometric element.

To balance the total viscous friction force within each geometric element, the local velocity vector around the i^{v}th vertex $\boldsymbol{v}_{i^{\mathrm{v}}}$ in Eq. (1) is defined as the mean velocity vector of the surrounding geometric elements:

$$\boldsymbol{v}_{i^{\mathrm{v}}} = \frac{\sum_{j^{\mathrm{e}}}^{\mathrm{element}} \eta_{j^{\mathrm{e}}} \boldsymbol{v}^{\mathrm{e}}_{j^{\mathrm{e}}} \delta_{i^{\mathrm{v}};j^{\mathrm{e}}}}{\sum_{j^{\mathrm{e}}}^{\mathrm{element}} \eta_{j^{\mathrm{e}}} \delta_{i^{\mathrm{v}};j^{\mathrm{e}}}}. \tag{14}$$

The viscous friction weight in each geometric element $\eta_{j^{\mathrm{e}}}$ is given by

$$\eta_{j^{\mathrm{e}}} = \begin{cases} \eta_{\mathrm{ec}} & \text{epithelial cells} \\ 0 & \text{extracellular space,} \end{cases} \tag{15}$$

where the constant η^{ec} denotes the viscous friction weights of cells.

The velocity of the j^{e}th geometric element $\boldsymbol{v}_{j^{\mathrm{e}}}$ is written as

$$\boldsymbol{v}_{j^{\mathrm{e}}} = \begin{cases} \dfrac{1}{n_{j^{\mathrm{e}}}} \sum_{k^{\mathrm{v}}}^{\mathrm{vertex}} \dfrac{d\boldsymbol{r}_{k^{\mathrm{v}}}}{dt} \delta_{k^{\mathrm{v}};j^{\mathrm{e}}} & \text{epithelial cells} \\ \boldsymbol{0} & \text{extracellular space,} \end{cases} \tag{16}$$

where $\sum_{k^{\mathrm{v}}}^{\mathrm{vertex}}$ sums the overall vertices.

4 Simulation of apoptosis-driven tissue morphogenesis

4.1 Numerical implementation and parameter setting

To solve Eq. (1), parameter values were normalized by unit length (l), unit time (τ), and unit energy (k_BT). Here, l and τ were set as $l = (v^{\mathrm{st}})^{\frac{1}{3}}$ and $\tau = 4\eta^{\mathrm{ec}} (v^{\mathrm{st}})^{\frac{2}{3}} / k_BT$. By focusing on some specific tissues, the physical parameters employed in the simulations can be determined based on those measured by experiments as described in (Okuda et al. 2015a). In this study, to establish that apoptotic cell behaviors could be successfully expressed by the proposed model, the half-life period of cells was varied by $\tau^{\mathrm{hl}} = 35$, 70, 140, 280, and 560.

Time integration of Eq. (1) was numerically performed using the improved Euler method with a time step of Δt. Local network patterns were reconnected when each edge included in a local pattern became shorter than a threshold value, Δl_{th}. Trials for applying the reconnection rule were conducted for each edge and each trigonal face at each time interval of Δt_r. All model parameters are shown in Table 1.

4.2 Tissue shrinkage driven by homogeneous cell apoptosis

To establish that successive cell apoptosis could be expressed by the proposed model, we simulated morphogenesis driven by homogeneous cell apoptosis. Here, to demonstrate the applicability of the proposed model to several multicellular structures, two typical topologies were employed for the initial conditions.

Condition I As an initial condition I, the cell aggregate has a structure of a spherical shell composed of a 3D monolayer cell sheet (Fig. 2c). The number of cells under this initial condition was set to $n^{\mathrm{c}}_0 = 999$. All cells randomly shift their phases from stable to apoptotic with a half-life of τ^{hl}.

Table 1 Model parameters

Symbol	Value (conditions I, I')	Value (conditions II, II')	Description
Physical parameters for cell mechanical properties			
k^{cv}	10		Constant of cell volume elasticity
κ^{cs}	0.2		Constant of cell surface energy
κ^{aj}	0.03	0.3	Constant of line energy at adherence junction
τ^{ap}	10		Time period of apoptotic phase
τ^{hl}	35 – 560		Half-life period of cells
v^{dis}	0.1		Constant of cell volume to disappear
Numerical parameters for computational simulations			
Δt	0.001		Integration time step
Δt_{r}	0.002		Time interval of network reconnections
Δl_{th}	0.05		Threshold length of network reconnections

Condition II As an initial condition II, the cell aggregate has a spherical structure composed of 3D compacted cells (Fig. 2d). The number of cells under this initial condition was set to $n_0^{\mathrm{c}} = 969$. All cells randomly shift their phases from stable to apoptotic with a half-life of τ^{hl}.

Under conditions I and II, apical surfaces (colored in orange in Figs. 2c and d) are defined as polygonal faces between boundary cells and the extracellular space outside the spherical tissue. To equilibrate the tissue morphology, tissue dynamics was calculated within a normalized period of 200 without cell shrinkage and disappearance.

Figure 3 shows the tissue dynamics induced by successive cell apoptosis. Figures 3a, b, f, and g show the whole and clip views of a shrinking tissue under conditions I and II (see also Movies 1 and 2 in the Supplemental data). Tissue morphology under conditions I and II shrank and remained rather spherical (Fig. 3a). In particular, the tissue morphology under condition I maintained the monolayer structure during morphogenesis (Fig. 3b). In addition, under conditions I and II, the global tissue shape is maintained to be spherical independent of the number of cells. This result suggests that homogeneous cell apoptosis could have a potential to control tissue size without affecting on tissue shape.

The graphs in Figs. 3c and h show the cell number as a function of time under conditions I and II, respectively. Colored lines in these graphs indicate the theoretical solution of Eq. (7). Under each condition of the half-life of τ^{hl}, the decreases in the number of cells obeyed the theoretical solution.

To establish that the proposed model could express apoptotic cell behaviors during tissue shrinkage, two basic quantities, cell volume and sphericity, representing cell size and shape were observed. Figures 3d and i show the average cell volumes during tissue shrinkage. Cell volumes were maintained at approximately $0.9v^{\mathrm{st}}$ during tissue shrinkage under all conditions of half-life period and tissue topology. Figures 3e and j show the average cell sphericities during tissue shrinkage. Cell sphericity is defined as the ratio of the radius of an equivalent sphere with the cell volume divided by that of the cell surface area. Cell sphericities were maintained at approximately 0.8 during tissue shrinkage under all conditions of apoptotic timing and tissue topology. These results correspond to the cell behaviors supposed in Sect. 3.2. Therefore, the proposed model successfully expresses cell behaviors as modeled.

4.3 Tissue deformation driven by region-specific cell apoptosis

To demonstrate effects of cell apoptosis on global tissue deformations, we simulated tissue deformations driven by cell apoptosis that occurs within a locally biased region. The employed initial condition is as follows.

Condition I' As an initial condition I', the cell aggregate has a structure of a spherical shell composed of a 3D monolayer cell sheet (Fig. 4a). The number of cells under this initial condition was set to $n_0^{\mathrm{c}} = 999$. Under condition I', the cells located in the fan-shaped region of $\pi/6$ radian from the z axis on the x-z plane as in Fig. 4a randomly shift their phases from stable to apoptotic with a half-life of τ^{hl} and the others maintain stable phases.

Under condition I', apical surface is defined on the boundary between cells and the space outside the tissue. To equilibrate the tissue morphology, tissue dynamics was calculated within a normalized period of 200 without cell shrinkage and disappearance.

Figure 4b shows the whole and clip views of tissue dynamics induced by region-specific apoptosis under condition I' (see also Movie 3 in the Supplemental data). Under condition I', the tissue locally shrunk by

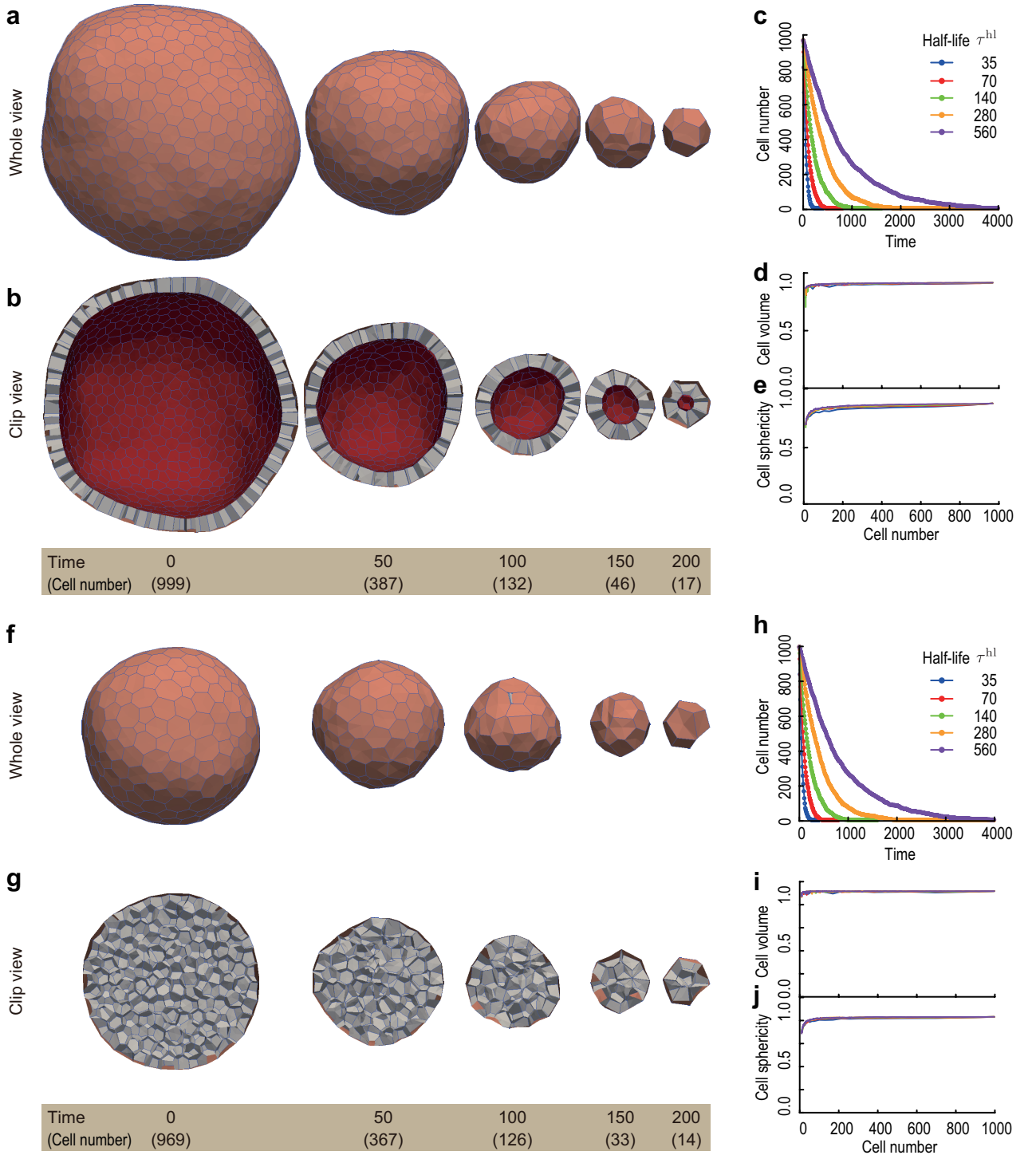

Fig. 3 Tissue shrinkage driven by homogeneous cell apoptosis. **a**, **f** Whole view of cell aggregates resulted from the initial conditions I and II with $\tau^{hl} = 35$, respectively. **b**, **g** Clip view of cell aggregates resulted from the initial conditions I and II at $\tau^{hl} = 35$, respectively. Snapshots of whole and clip views of tissues at $t = 0$, 50, 100, 150, and 200 (in order from left). The tissue under condition I includes cell numbers $n^c = 999$, 387, 132, 46, and 17 [blue dots in (**c**)]. The tissue under condition II includes cell numbers $n^c = 969$, 367, 126, 33, and 14 [blue dots in (**h**)]. The morphogenetic processes under conditions I and II with $\tau^{hl} = 560$ are also shown in Movies 1 and 2 in the Supplemental data, respectively. **c**, **h** Number of cells as a function of time under conditions I and II. **d**, **i** Cell volume as a function of the number of cells under conditions I and II. **e**, **j** Cell sphericity as a function of the number of cells under conditions I and II. Colored dots in (**c**), (**d**), (**e**), (**h**), (**i**), and (**j**) indicate the following conditions: $\tau^{hl} = 35$ (blue), 70 (red), 140 (green), 280 (orange), and 560 (purple). Colored lines indicate the theoretical solutions of Eq. (7).

region-specific apoptosis. Because the tissue has a structure of continuous sheet, the local cell apoptosis caused the global tissue bending by pulling on surrounding cells.

4.4 Cell rearrangements driven by region-specific cell apoptosis

To establish that successive cell apoptosis and rearrangements could be expressed by the proposed model, we performed further simulations of morphogenesis driven by region-specific cell apoptosis. Because region-specific cell apoptosis is often observed in embryogenesis (Fekete et al. 1997; Trousse et al. 2001; Kuan et al. 2000; Suzanne and Steller 2013; Zhao and Rivkees 2000), it has biological as well as numerical importance to apply the proposed model to the morphogenesis driven by region-specific cell apoptosis. The employed initial condition is as follows.

Condition II' As an initial condition II', the cell aggregate has a spherical structure composed of 3D compacted cells (Fig. 5a). The number of cells under this initial condition was set to $n_0^{\mathrm{c}} = 969$. Under condition II', the cells located on the surface randomly shift their phases from stable to apoptotic with a half-life of τ^{hl} and the others maintain stable phases.

Under condition II', apical surfaces (colored in orange in Fig. 5a) are defined as polygonal faces between boundary cells and the extracellular space outside the spherical tissue. To equilibrate the tissue morphology, tissue dynamics was calculated within a normalized period of 200 without cell shrinkage and disappearance.

Figure 5b shows the clip views of tissue dynamics induced by region-specific apoptosis under condition II' (see also Movie 4 in the Supplemental data). Under condition II', successive cell apoptosis on the surface drive successive, directional cell movements from the inside to the surface within the 3D cell aggregate. In the simulations under condition II', while the tensile force on adherence junction maintains the cell aggregate to be spherical, the number of cells on the surface of the aggregate decreases due to cell apoptosis. Hence, to fill in the space of apoptotic cells, the cells in the inside of the aggregate directionally moves to the surface. This result shows that the proposed model successfully expresses successive cell rearrangements without any topological errors.

5 Discussion

5.1 Expression of apoptotic cell behaviors based on a RNR framework

In the simulations under conditions I and II, tissues shrank, where the number of cells decreased and cell size and shape were maintained (Fig. 3). This tendency is similar to those observed under all of the employed conditions with apoptotic timing and tissue topology. These results correspond to the employed conditions of cell behaviors described in Section 3. Moreover, the tissue shrinkage under conditions I' and II' involved local tissue deformations and successive cell rearrangements from the inside to the surface within the 3D cell aggregate (Figs. 4 and 5). These apoptosis-driven dynamics did not include any topological errors. Thus, the proposed model successfully expresses apoptotic cell behaviors based on the RNR model framework.

In epithelia, cell apoptosis includes apical constriction, extrusion from epithelium, blebbing, and cell fragmentation. On the other hand, in this study, the process of cell apoptosis was simplified to be the volume decrease and disappearance of cells. In this model, the apical constriction can be expressed using an effective energy function. Moreover, by representing epithelial cells as well as external tissues, the extrusion from epithelium to external tissues can be expressed by cell rearrangements. In case of representing epithelial cells without external tissues, the extrusion process can be also implicitly expressed by the volume decrease and disappearance of apoptotic cells. However, it seems difficult to express the blebbing and cell fragmentation in this model because of the limitation of the expressible length scale. By focusing on the change in apoptotic cell volume, the merging process in the model can be interpreted as the process of the end of cell extrusion or the loss of the fragmented cellular components. Therefore, the proposed model expresses apoptotic cell behaviors such as cellular volume decrease and apical constriction, as well as the cell extrusion from epithelium.

To model cell disappearance, it seems more admissible that a polyhedron disappears at the position of its centroid, whereas in the proposed model the polyhedron is merged into the other polyhedron. Because an apoptotic cell disappears at the volume of v_{dis}, the drift caused by merging polyhedrons is estimated to be in the order of $(v_{\mathrm{dis}})^{1/3}$ that is a scale of cell–cell boundary face. To minimize the drift, locations of the vertices composing apoptotic polyhedrons are modified using Eq. (6). This modification maintains the centroid of surrounding cells but not the local strain. The strain is also in the order of cell–cell boundary face,

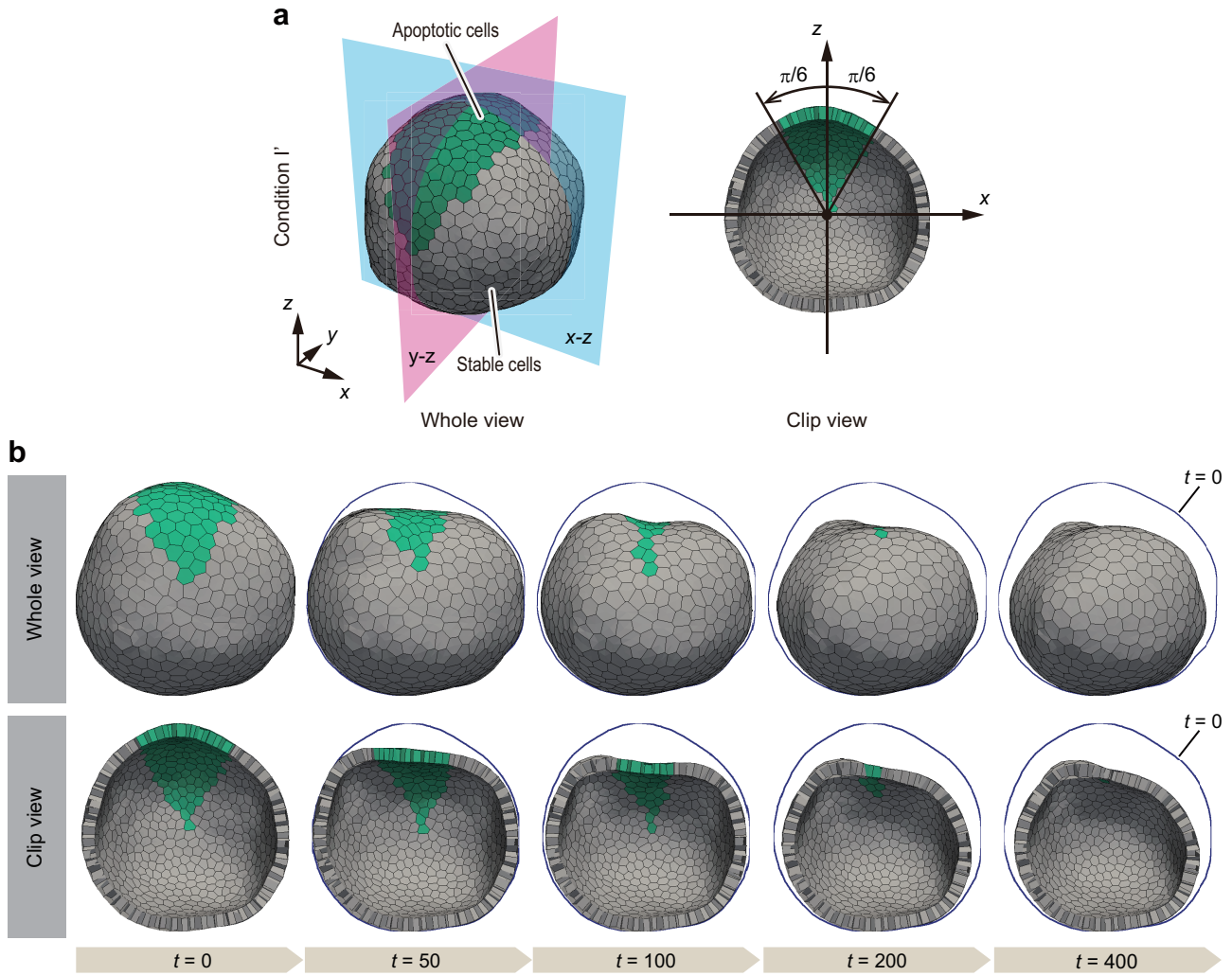

Fig. 4 Tissue deformation driven by region-specific cell apoptosis. **a** Whole and clip views of the initial structure of the cell aggregate under condition I'. The cell aggregate has a structure of spherical shell composed of 3D monolayer cell aggregate. The outside surface of the cell aggregate is apical. At $t = 0$, the cells located in the fan-shaped region between $-\pi/6$ and $\pi/6$ radian from the tissue centroid on the x-z plane (green) are set to be apoptotic cells, which shift their phases from stable to apoptotic, and the other cells (gray) maintain stable phases. **b** Tissue deformation of the 3D monolayer cell aggregate. Top and bottom slides present the whole and clip views of cell aggregates resulting from condition I' with $\tau^{\mathrm{hl}} = 560$. Snapshots of these tissues are at $t = 0$, 50, 100, 200, and 400 (in order from left). Blue lines represent the outlines of tissues at $t = 0$. The morphogenetic process is also shown in Movie 3 in the Supplemental data.

which immediately relaxes within a time scale of individual cell deformations. Therefore, the proposed model properly expresses coarse-grained behaviors of apoptotic cells above the scale larger than individual cells.

5.2 Anticipated applications of the proposed model

In the simulations performed using the proposed model, by assuming that the apoptotic timing was independent of cell mechanical states, we determined the timing of the phase shift from stable to apoptotic and timing of the disappearance (described in Section 2.2). Generally, this assumption was not always essential for the proposed model. We emphasize that the timing of cell apoptosis is entirely arbitrary. Thus, the proposed model could be applied to various behaviors of cell apoptosis by regulating the timing. For instance, simultaneous cell apoptosis can be expressed by using the same timing of the phase shift and period of the apoptotic phase among multiple cells.

The simulations expressed the time variance of cell mechanical properties and reference states (described in Section 3.2); however, they can be expressed in detail on the basis of a different time scale. For example,

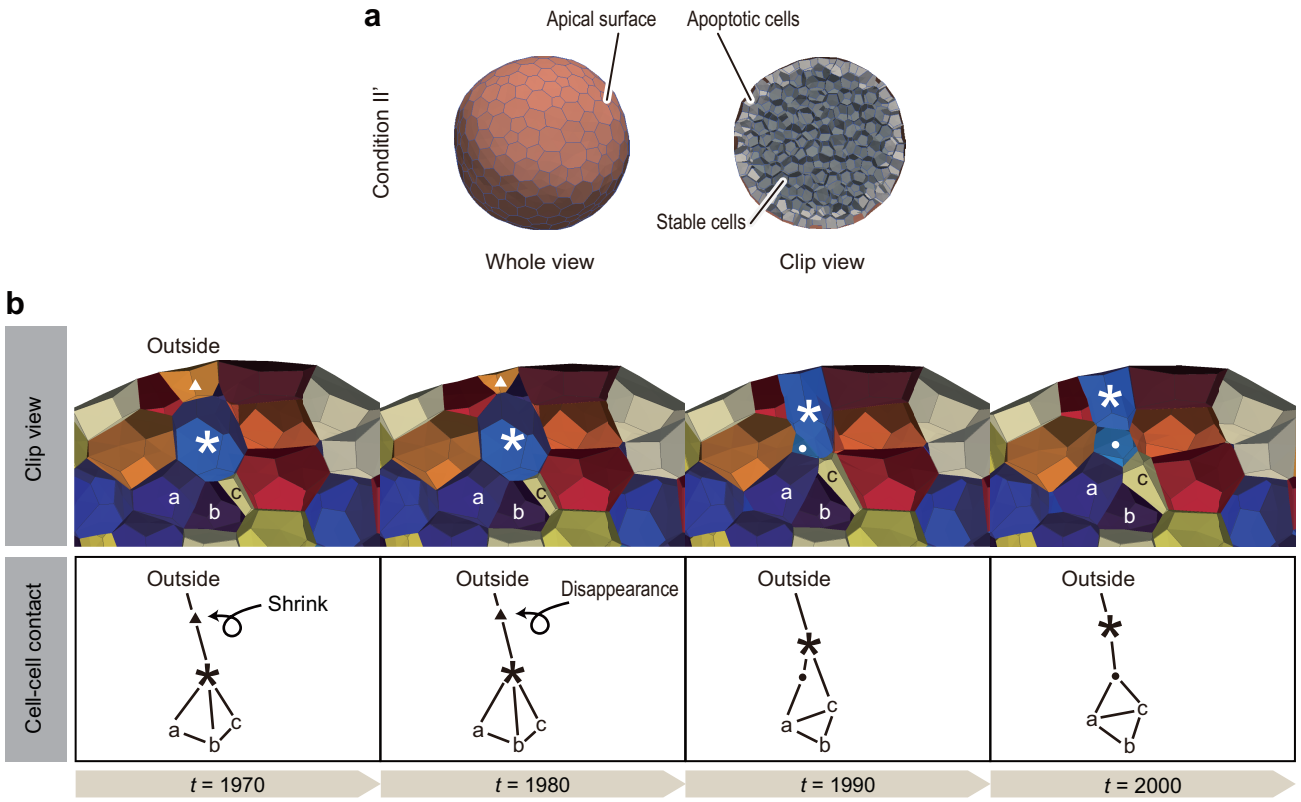

Fig. 5 Cell rearrangements driven by region-specific cell apoptosis. **a** Whole and clip views of the initial structure of the cell aggregate under condition II'. The cell aggregate has a spherical structure composed of 3D compacted cell aggregates. The outside surfaces of the individual cell aggregates (orange) are apical. In the aggregate, the cells located on the surface (light gray) shift their phases from stable to apoptotic, and the other cells (dark gray) maintain stable phases. **b** Directional cell rearrangements from the inside to the surface within the 3D compacted cell aggregate. Top slides present the clip view of cell aggregates resulting from condition II' with $\tau^{\mathrm{hl}} = 560$ focusing on the cell movements around the tissue surface. Snapshots of these tissues are at $t = 1970$, 1980, 1990, and 2000 (in order from left). The morphogenetic process is also shown in Movie 4 in the Supplemental data. Bottom slides present a cell–cell contact relationship within the respective tissue of the above clip view. The cell marked by (▲) shrank from $t = 1970$ to 1980 and disappeared from $t = 1980$ to 1990. Simultaneously, the cells marked by (∗) and (b) departed from each other, and cells marked by (a) and (c) made contact. The cell marked by (·) appeared between the cells marked by (∗) and (a) at $t = 1980$, and it was stuck in between the cells marked by (∗) and (c).

cell shrinkage is accompanied by the decreases in cell volume and in apical surface and/or apicobasal height (Toyama et al. 2008; Teng and Toyama 2011; Monier et al. 2015). Moreover, during cell apoptosis in epithelium, adhesive interactions among neighboring cells dynamically change so as to cause the cell extrusion from epithelium to surrounding tissues. During these processes, cell mechanical properties and reference states vary progressively over time. These details can be reflected by choosing proper potential energy functions $U(\{t_{j^c}\})$ in Eq. (8).

In addition, mechanical feedback in apoptotic cell behaviors may play an important role during multicellular morphogenesis. Active stress generated by cell activities, such as pushing forces induced by cell proliferation in epithelial sheets, is transferred to surrounding cells. The surrounding cells may be provided with a feedback signal that regulates cell apoptosis because of this stress (Milan et al. 1997). This mechanical feedback system may cause cell competition on the basis of the mechanical force balance among cells. A previous study reported that, in the proposed model, a mechanical feedback system could also be implemented by coupling the apoptotic cell behaviors with cell mechanical states and with the intercellular molecular signaling (Okuda et al. 2015b).

5.3 Limitation and applicability

In principle, detailed expressions of apoptotic cell behaviors at the subcellular scale are limited in the proposed model; for example, during apoptosis, cell mechanical properties become inhomogeneous at the subcellular scale because of the oriented configurations of

stress fibers and localized actomyosins. These inhomogeneities in mechanical properties at the subcellular scale cannot be expressed because the proposed model can only express apoptotic cell behaviors over a range of length scales no larger than a polygonal face, the minimum unit comprising cell shapes in the RNR model. Therefore, the mechanical properties and states in the subcellular scale should be coarse-grained into those at the minimum scale of the RNR model. For example, effects of apical constriction during apoptosis could be expressed by introducing a potential energy that decreases the contour length of a apical polygonal face as described by (Farhadifar et al. 2007). Thus, by designing the potential energy function, the proposed model permits an analysis of the mechanism by which subcellular inhomogeneities affect 3D multicellular morphogenesis.

5.4 Future perspectives

The proposed model will help to understand the mechanics of 3D multicellular morphogenesis involving cell apoptosis, particularly, the cause-effect relationships between single cell dynamics and morphogenesis. The proposed model is a powerful approach to address how apoptotic cell behaviors affect 3D multicellular morphogenesis at a scale of single cell. Understanding these functions of cell apoptosis is necessary to better understand morphogenesis, and this will be useful as fundamental knowledge for controlling morphogenesis in tissue engineering (Asally et al. 2012). Furthermore, general validation of the proposed model warrants certain predictions for the morphogenetic processes of 3D tissues and organs. Therefore, the proposed model will contribute to exploring the frontiers of developmental biomechanics.

6 Conclusions

To analyze the mechanical effects of apoptotic cell behaviors of cell shrinkage and disappearance on multicellular morphogenesis, we modeled cell apoptosis based on a RNR model framework. In this model, cell shrinkage was expressed by potential energy as a function of individual cell times. In addition, cell disappearance was expressed by merging a polyhedron representing the apoptotic cell with the neighboring polyhedron. The apoptotic cell behaviors were characterized by two parameters of the timing: the timing of the phase shift from stable to apoptotic and the timing of the disappearance. To establish that apoptotic cell behaviors can be expressed, the apoptosis-driven dynamics of cell aggregates was simulated. As a result, cell aggregates shrank with time, wherein the number of cells decreased and the average cell size and shape were maintained. Furthermore, region-specific apoptosis caused the global tissue bending as well as successive, directional cell rearrangements. From these results, the proposed model successfully expressed apoptotic cell behaviors based on the RNR model framework. Using the proposed model, we attempted to determine the general effects of apoptotic cell behaviors on 3D multicellular morphogenesis at a scale of single cell.

Acknowledgements We appreciate Dr. Eri Kuranaga from RIKEN Center for Developmental Biology for her valuable comments. This work was supported by JSPS KAKENHI Grant Number 15K14534.

References

Asally M, Kittisopikul M, Rue P, Du Y, Hu Z, Caátay T, Robinson AB, Lu H, Garcia-Ojalvo J, Suel GM (2012). “Localized cell death focuses mechanical forces during 3D patterning in a biofilm.” Proc Natl Acad Sci U S A. 109(46): 18891-18896.

Davies JA (2005). “Mechanisms of morphogenesis: the creation of biological form.” Elsevier Academic Press, Burlington, New York.

Farhadifar R, Röper JC et al (2007). “The influence of cell mechanics, cell–cell interactions, and apoptosis on epithelial packing.” Curr Biol 17(24): 2095-2104.

Fekete DM, Homburger SA, Waring MT, Riedl AE, Garcia LF (1997). “Involvement of programmed cell death in morphogenesis of the vertebrate inner ear.” Development. 124(12): 2451-2461.

Friedlander DR, Mège RM et al (1989). “Cell sorting-out is modulated by both the specificity and amount of different cell-adhesion molecules (CAMs) expressed on cell-surfaces.” Proc Natl Acad Sci U S A 86(18): 7043-7047.

Honda H, Motosugi N et al (2008). “Computer simulation of emerging asymmetry in the mouse blastocyst.” Development 135(8): 1407-1414.

Honda H, Nagai T et al (2008). “Two different mechanisms of planar cell intercalation leading to tissue elongation.” Dev Dyn 237(7): 1826-1836.

Honda H, Tanemura M et al (2004). “A three-dimensional vertex dynamics cell model of space-filling polyhedra simulating cell behavior in a cell aggregate.” J Theor Biol 226(4): 439-453.

Ingber DE, Mammoto T (2010). “Mechanical control of tissue and organ development.” Development 137(9): 1407-1420.

Kuan CY, Roth KA, Flavell RA, Rakic P (2000). "Mechanisms of programmed cell death in the developing brain." Trends Neurosci 23(7): 291-297.

Kuranaga E, Matsunuma T, Kanuka H, Takemoto K, Koto A, Kimura K, Miura M (2011). "Apoptosis controls the speed of looping morphogenesis in Drosophila male terminalia." Development 138(8): 1493-1499.

Lecuit T, Lenne PF (2007). "Cell surface mechanics and the control of cell shape, tissue patterns and morphogenesis." Nat Rev Mol Cell Biol 8(8): 633-644.

Lecuit T, Rauzi M et al (2008). "Nature and anisotropy of cortical forces orienting Drosophila tissue morphogenesis." Nat Cell Biol 10(12): 1401-1410.

Lecuit T, Rauzi M et al (2010). "Planar polarized actomyosin contractile flows control epithelial junction remodeling." Nature 468(7327): 1110-1114.

Milan M, Campuzano S, Garcia-Bellido A (1997). "Developmental parameters of cell death in the wing disc of Drosophila." Proc Natl Acad Sci U S A. 94(11): 5691-5696.

Monier B, Gettings M, Gay G, Mangeat T, Schott S, Guarner A, Suzanne M (2015). "Apico-basal forces exerted by apoptotic cells drive epithelium folding." Nature 518(7538): 245-248.

Okuda S, Inoue Y, Eiraku M, Sasai Y, Adachi T (2013a). "Reversible network reconnection model for simulating large deformation in dynamic tissue morphogenesis. Biomech Model Mechanobiol 12(4): 627-644.

Okuda S, Inoue Y, Eiraku M, Sasai Y, Adachi T (2013b). "Modeling cell proliferation for simulating three-dimensional tissue morphogenesis based on a reversible network reconnection framework." Biomech Model Mechanobiol 12(5): 987-996.

Okuda S, Inoue Y, Eiraku M, Sasai Y, Adachi T (2013c). "Apical contractility in growing epithelium supports robust maintenance of smooth curvatures against cell-division-induced mechanical disturbance." J Biomech 46(10): 1705-1713.

Okuda S, Inoue Y, Eiraku M, Adachi T, Sasai Y (2015a). "Vertex dynamics simulations of viscosity-dependent deformation during tissue morphogenesis." Biomech Model Mechanobiol 14(2): 413-425.

Okuda S, Inoue Y, Watanabe T, Adachi T (2015b). "Coupling intercellular molecular signaling with multicellular deformation for simulating three-dimensional tissue morphogenesis." Interface Focus 5(2): 20140095.

Okuda S, Inoue Y, Adachi T (2015c). "Three-dimensional vertex model for simulating multicellular morphogenesis." Biophysics and Physicobiology 12: 13-20.

Rauzi M, Verant P et al (2008). "Nature and anisotropy of cortical forces orienting Drosophila tissue morphogenesis." Nat Cell Biol 10(12): 1401-1410.

Saias L, Swoger J, D'Angelo A, Hayes P, Colombelli J, Sharpe J, Salbreux G, Solon J. (2015). " Decrease in cell volume generates contractile forces driving dorsal closure." Dev Cell 33(5):611-621.

Staple DB, Farhadifar R et al (2010). "Mechanics and remodeling of cell packings in epithelia." Eur Phys J E Soft Matter 33(2): 117-127.

Suzanne M, Steller H (2013). "Shaping organisms with apoptosis." Cell Death Differ 20(5): 669-675.

Teng X, Toyama Y (2011). "Apoptotic force: active mechanical function of cell death during morphogenesis." Dev Growth Differ 53(2): 269-276.

Toyama Y, Peralta XG, Wells AR, Kiehart DP, Edwards GS (2008). "Apoptotic force and tissue dynamics during Drosophila embryogenesis." Science 321(5896): 1683-1686.

Trousse F, Esteve P, Bovolenta P (2001). "Bmp4 mediates apoptotic cell death in the developing chick eye." J Neurosci 21(4): 1292-1301.

Weliky M, Oster G (1990). "The mechanical basis of cell rearrangement. I. Epithelial morphogenesis during fundulus epiboly." Development 109(2): 373-386.

Woolner S, Papalopulu N (2012). "Spindle Position in Symmetric Cell Divisions during Epiboly Is Controlled by Opposing and Dynamic Apicobasal Forces." Dev Cell 22(4): 775-787.

Yamaguchi Y, Shinotsuka N, Nonomura K, Takemoto K, Kuida K, Yosida H, Miura M (2011). " Live imaging of apoptosis in a novel transgenic mouse highlights its role in neural tube closure." J Cell Biol 195(6): 1047-1060.

Zhao Z, Rivkees SA (2000). "Programmed cell death in the developing heart: regulation by BMP4 and FGF2." Dev Dyn 217(4): 388-400.